

Optimizing Layout of a Planar Wire-Actuated Parallel Manipulator Based on Stiffness and Failure Analyses

Amir Moradi¹, Leila Notash²

¹Department of Mechanical and Materials Engineering, Queen's University, moradi@me.queensu.ca

²Department of Mechanical and Materials Engineering, Queen's University, notash@me.queensu.ca

Abstract

In this paper, stiffness of a planar wire-actuated parallel manipulator with two degrees of freedom is studied. In this manipulator, three wire actuators are used to provide two translations. The complete form of the stiffness matrix of the manipulator is formulated parametrically using the differential form of the static force balance equations for a given position of the manipulator. Failure of a wire (when wire is disconnected) and its effect on the stiffness of the manipulator are investigated. Stiffness maps of the manipulator over the workspace are developed before and after failure, also with and without considering the desired stiffness bound. Optimum layouts of the manipulator are identified using the genetic algorithm to maximize the area of the stiffness maps.

Keywords: Wire-actuated parallel manipulators, stiffness map, failure analysis, optimum layout

1. INTRODUCTION

In this paper a planar wire-actuated parallel manipulator with two degrees of freedom (DOF) is considered. Mobile platform of the wire-actuated manipulator is attached to the base with multiple wires. The light weight of wire actuators and easy assembly, disassembly and transportation of the manipulator are some of the advantages of wire-actuated manipulators. In [1], design of a wire-actuated manipulator for ultrahigh speed motion was studied based on stiffness analysis. Wires can be used only when they are in tension. Thus, keeping the positive tension in wires is a challenge. Therefore, in the absence of gravity, at least $n + 1$ wires are required in the design of a fully controllable n -DOF manipulator.

Because of using the wires, the stiffness of wire-actuated manipulators is relatively low, hence stiffness analysis is necessary. The stiffness of manipulators can be used as an index of the accuracy in the static case at the position and force levels, and for optimum design of manipulators. For example, the optimum design of the 3-DOF spherical parallel manipulators based on the conditioning and stiffness indices was studied in [2]. In [3], a conceptual design of variable stiffness elements using wire-actuated mechanisms was presented.

Stiffness matrix transforms a differential displacement of the end effector of a manipulator into the corresponding incremental change in the applied force and moment on its end effector [4-6].

Stiffness matrix of the planar manipulator is symmetric when it is formulated with respect to a reference frame which is located at the end effector and has the orientation of the fixed base frame [6]. In the calculation of the stiffness matrix, the fixed point on the mobile platform that undergoes the displacement increment and the point of application of the forces applied on the mobile platform are coincident [7].

In [8], the mechanical failures of parallel and serial manipulators were presented and classified. A failure recovery methodology for wire-actuated parallel manipulators was studied in [9]. The set of wrenches that a wire-actuated manipulator with point mass mobile platform can apply to its surroundings was studied in [10] and it was used to analyze the type of failure that would occur in the manipulator. In [11], the effect of failure of a wire on stiffness maps of planar wire-actuated parallel manipulators was investigated.

Knowledge of optimum layout of a manipulator can be used in design and control of the manipulator. For instance, the lost stiffness of wire-actuated parallel manipulators after failure of a wire can be retrieved partially by changing the anchor positions of the manipulator.

The optimum layouts of 2-DOF planar wire-actuated manipulators are introduced in this paper, i.e., optimum anchor positions are identified using the genetic algorithm to maximize the area of the stiffness map before and after failure. The stiffness modelling and failure of a wire in the manipulator, when wire is disconnected, will be reviewed in Section 2. The stiffness maps for the manipulator before and after the failure will be developed in Section 3. In Section 4, the optimum layouts of the manipulator will be introduced. The conclusion of article will be in Section 5.

2. MODELLING

Figure 1 shows the parameters and reference frame of the planar translational wire-actuated parallel manipulator. Coordinate system $\Psi(X,Y)$ is attached to the base at point 0. The wire is released from a spool attached to an electric motor. A pulley is placed at anchor points A_i between the spool of wire i and its attachment point on the mobile platform as shown in Figure 1. The constant length of wire between the motor spool and the pulley is l_c . The variable length of wire between the pulley and the attachment point on the mobile platform is l_i , which is obtained from the inverse kinematic analysis of the manipulator. The vector of tension in wire i is τ_i and the anchor points A_i can move on a circular rail shown by dashed-line in Figure 1. It should be noted that the mobile platform is a point mass. Given the position vector of the mobile platform $\mathbf{p} = [p_x, p_y]^T$ and the position vector of anchor A_i , $\mathbf{a}_i = [a_{ix}, a_{iy}]^T$, wire orientation α_i and wire length l_i are formulated as

$$l_i = \sqrt{(a_{ix} - p_x)^2 + (a_{iy} - p_y)^2} \quad (1)$$

$$\alpha_i = \text{atan2}((a_{iy} - p_y)/(a_{ix} - p_x)) \quad (2)$$

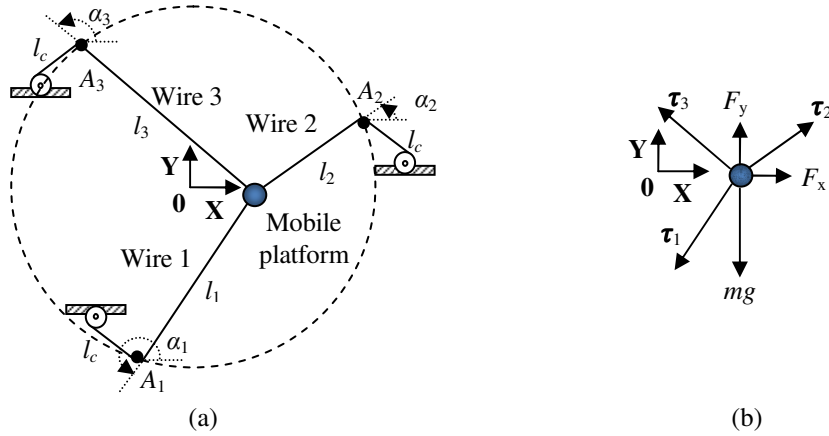


Figure 1. (a) Coordinate and variables of 2-DOF planar three-wire-actuated parallel manipulator, (b) free body diagram of mobile platform.

The Jacobian matrix of the manipulator in terms of the wire orientations is formulated as

$$\mathbf{J} = - \begin{bmatrix} \cos \alpha_1 & \sin \alpha_1 \\ \cos \alpha_2 & \sin \alpha_2 \\ \cos \alpha_3 & \sin \alpha_3 \end{bmatrix} \quad (3)$$

where

$$\sin \alpha_i = \frac{a_{iy} - p_y}{\sqrt{(a_{ix} - p_x)^2 + (a_{iy} - p_y)^2}} \quad (4)$$

$$\cos \alpha_i = \frac{a_{ix} - p_x}{\sqrt{(a_{ix} - p_x)^2 + (a_{iy} - p_y)^2}} \quad (5)$$

The static force balance for the manipulator can be written as

$$\mathbf{F} = \mathbf{J}^T \boldsymbol{\tau} \quad (6)$$

where $\boldsymbol{\tau} = [\tau_1, \tau_2, \tau_3]^T$ is the vector of wire tensions. Vector $\mathbf{F} = [F_x, F_y - mg]^T$ corresponds to the Cartesian forces applied on the mobile platform, which is also called the wrench acting on the mobile platform. It should be noted that the mass of mobile platform m is constant. To calculate the stiffness matrix, equation (6) is differentiated as

$$\delta \mathbf{F} = \begin{bmatrix} \delta F_x \\ \delta F_y \end{bmatrix} = \delta \mathbf{J}^T \boldsymbol{\tau} + \mathbf{J}^T \delta \boldsymbol{\tau} \quad (7)$$

Stiffness matrix can be formulated by re-arranging equation (7) as

$$\delta \mathbf{F} = \begin{bmatrix} \delta F_x \\ \delta F_y \end{bmatrix} = \mathbf{K} \begin{bmatrix} \delta p_x \\ \delta p_y \end{bmatrix} \quad (8)$$

The first term on the right-hand side of equation (7) can be expanded as

$$\delta \mathbf{J}^T \boldsymbol{\tau} = \sum_{i=1}^n \delta \mathbf{J}_i^T \tau_i \quad (9)$$

where \mathbf{J}_i^T is the i th column of matrix \mathbf{J}^T , and for the manipulator the transpose of the Jacobian matrix is in terms of the wire orientation α_i . Thus, $\delta \mathbf{J}_i^T$ can be written as

$$\delta \mathbf{J}_i^T = \frac{\partial \mathbf{J}_i^T}{\partial \alpha_i} \delta \alpha_i \quad (10)$$

A relationship between the differential of wire orientations $\delta\boldsymbol{\alpha} = [\delta\alpha_1, \dots, \delta\alpha_3]^T$ and the twist vector could also be derived. The mobile platform pose in terms of the parameters of wire i can be written as

$$\begin{bmatrix} x \\ y \end{bmatrix} = \begin{bmatrix} a_{i_x} - l_i \cos \alpha_i \\ a_{i_y} - l_i \sin \alpha_i \end{bmatrix}, \quad i=1, \dots, 3 \quad (11)$$

By taking the derivative of equation (11), a relationship for the vector of wire orientations $\delta\boldsymbol{\alpha}$ in terms of the twist vector is derived as

$$\delta\boldsymbol{\alpha} = \mathbf{A} \begin{bmatrix} \delta p_x \\ \delta p_y \end{bmatrix} \quad (12)$$

where

$$\mathbf{A} = \begin{bmatrix} \frac{\sin \alpha_1}{l_1} & -\frac{\cos \alpha_1}{l_1} \\ \frac{\sin \alpha_2}{l_2} & -\frac{\cos \alpha_2}{l_2} \\ \frac{\sin \alpha_3}{l_3} & -\frac{\cos \alpha_3}{l_3} \end{bmatrix} \quad (13)$$

Considering the Jacobian matrix given in equation (3), $\delta\mathbf{J}_i^T$ can be written in terms of vector $\delta\boldsymbol{\alpha} = [\delta p_x, \delta p_y]^T$ as

$$\delta\mathbf{J}_1^T = \begin{bmatrix} \sin \alpha_1 & 0 & 0 \\ -\cos \alpha_1 & 0 & 0 \end{bmatrix} \mathbf{A} \delta\boldsymbol{\alpha} \quad (14)$$

$$\delta\mathbf{J}_2^T = \begin{bmatrix} 0 & \sin \alpha_2 & 0 \\ 0 & -\cos \alpha_2 & 0 \end{bmatrix} \mathbf{A} \delta\boldsymbol{\alpha} \quad (15)$$

$$\delta\mathbf{J}_3^T = \begin{bmatrix} 0 & 0 & \sin \alpha_3 \\ 0 & 0 & -\cos \alpha_3 \end{bmatrix} \mathbf{A} \delta\boldsymbol{\alpha} \quad (16)$$

For wire-actuated parallel manipulators, the stiffness of each wire is modelled as a simple spring. Thus, the changes in wire forces is written as

$$\delta\boldsymbol{\tau} = \mathbf{K}_q \boldsymbol{\delta} \quad (17)$$

where

$$\mathbf{K}_q = \text{diag}[k_1, k_2, k_3] \quad (18)$$

The term k_i , $i = 1, \dots, 3$, is the stiffness constant for the i th wire actuator. The Jacobian matrix of equation (3) gives the relationship between the vector of differential change in wire lengths $\boldsymbol{\delta} \mathbf{l} = [\delta l_1, \dots, \delta l_3]^T$ and the vector of differential form of twist as

$$\boldsymbol{\delta} \mathbf{l} = \mathbf{J} \delta\boldsymbol{\alpha} \quad (19)$$

Upon substituting equation (19) in equation (17), the relationship for $\delta\boldsymbol{\tau}$ in terms of the infinitesimal motion is obtained as

$$\delta\boldsymbol{\tau} = \mathbf{K}_q \mathbf{J} \delta\boldsymbol{\alpha} \quad (20)$$

Thus, the second term on the right-hand side of equation (6) can be written as

$$\mathbf{J}^T \delta\boldsymbol{\tau} = \mathbf{J}^T \mathbf{K}_q \mathbf{J} \delta\boldsymbol{\alpha} \quad (21)$$

Stretch of the wire ΔL under the effect of an axial load F is calculated as [12]

$$\Delta L = \frac{FL}{EA_w} \quad (22)$$

where L is the length of the wire; E is the equivalent Young's modulus of elasticity of the wire, which can be identified by tension test; and A_w is the cross-sectional area of the wire, where $A_w = \pi D^2/4$ and D is the nominal (outer) diameter of the wire and can be measured by caliper. The length of wire i for a given position of the mobile platform is $l_i + l_c$. The stiffness of wire i , k_i , which varies with the wire length, is formulated as

$$k_i = \frac{E_i A_{wi}}{l_i + l_c} \quad (23)$$

where E_i is the Young's modulus of elasticity of the wire and A_{wi} is its cross-sectional area. The complete form of the stiffness matrix of the manipulator is derived as

$$\mathbf{K} = \begin{bmatrix} k_{11} & k_{12} \\ k_{21} & k_{22} \end{bmatrix} = \mathbf{J}^T \mathbf{K}_q \mathbf{J} + \tau_1 \begin{bmatrix} \sin \alpha_1 & 0 & 0 \\ -\cos \alpha_1 & 0 & 0 \end{bmatrix} \mathbf{A} + \tau_2 \begin{bmatrix} 0 & \sin \alpha_2 & 0 \\ 0 & -\cos \alpha_2 & 0 \end{bmatrix} \mathbf{A} + \tau_3 \begin{bmatrix} 0 & 0 & \sin \alpha_3 \\ 0 & 0 & -\cos \alpha_3 \end{bmatrix} \mathbf{A} \quad (24)$$

$$k_{11} = \frac{E_1 A_{w1} \cos^2 \alpha_1}{l_1 + l_c} + \frac{E_2 A_{w2} \cos^2 \alpha_2}{l_2 + l_c} + \frac{E_3 A_{w3} \cos^2 \alpha_3}{l_3 + l_c} + \frac{\sin^2 \alpha_1 \tau_1}{l_1} + \frac{\sin^2 \alpha_2 \tau_2}{l_2} + \frac{\sin^2 \alpha_3 \tau_3}{l_3} \quad (25)$$

$$k_{12} = k_{21} = \frac{E_1 A_{w1} \cos \alpha_1 \sin \alpha_1}{l_1 + l_c} + \frac{E_2 A_{w2} \cos \alpha_2 \sin \alpha_2}{l_2 + l_c} + \frac{E_3 A_{w3} \cos \alpha_3 \sin \alpha_3}{l_3 + l_c} - \frac{\cos \alpha_1 \sin \alpha_1 \tau_1}{l_1} - \frac{\cos \alpha_2 \sin \alpha_2 \tau_2}{l_2} - \frac{\cos \alpha_3 \sin \alpha_3 \tau_3}{l_3} \quad (26)$$

$$k_{22} = \frac{E_1 A_{w1} \sin^2 \alpha_1}{l_1 + l_c} + \frac{E_2 A_{w2} \sin^2 \alpha_2}{l_2 + l_c} + \frac{E_3 A_{w3} \sin^2 \alpha_3}{l_3 + l_c} + \frac{\cos^2 \alpha_1 \tau_1}{l_1} + \frac{\cos^2 \alpha_2 \tau_2}{l_2} + \frac{\cos^2 \alpha_3 \tau_3}{l_3} \quad (27)$$

Having the expressions for the entries of the stiffness matrix, this matrix can be calculated for every position of the mobile platform inside the workspace in order to develop the stiffness maps.

The manipulator studied in this paper is a three-wire-actuated parallel manipulator with one degree of actuation redundancy, i.e., three wire actuators are used to provide translations along X and Y directions.

According to the static force balance equation, wire tensions are formulated in terms of the vector of force \mathbf{F} , generalized-inverse of the transposed Jacobian matrix \mathbf{J}^T and vector \mathbf{N} which corresponds to the orthonormal basis for the null space of the transposed Jacobian matrix.

$$\boldsymbol{\tau} = \mathbf{J}^{T\#} \mathbf{F} + \lambda \mathbf{N} \quad (28)$$

where λ is an arbitrary scalar for the manipulator studied in this paper.

$$\tau_1 = \frac{(2 \cos \alpha_1 - \cos(\alpha_1 - 2\alpha_2) - \cos(\alpha_1 - 2\alpha_3))F_x + (2 \sin \alpha_1 + \sin(\alpha_1 - 2\alpha_2) + \sin(\alpha_1 - 2\alpha_3))(F_y - mg)}{\cos(2(\alpha_1 - \alpha_2)) + \cos(2(\alpha_1 - \alpha_3)) + \cos(2(\alpha_2 - \alpha_3)) - 3} - \lambda \frac{\sin(\alpha_2 - \alpha_3)}{\sin(\alpha_1 - \alpha_2)} \quad (29)$$

$$\tau_2 = \frac{(2 \cos \alpha_2 - \cos(\alpha_2 - 2\alpha_1) - \cos(\alpha_2 - 2\alpha_3))F_x + (2 \sin \alpha_2 + \sin(\alpha_2 - 2\alpha_1) + \sin(\alpha_2 - 2\alpha_3))(F_y - mg)}{\cos(2(\alpha_1 - \alpha_2)) + \cos(2(\alpha_1 - \alpha_3)) + \cos(2(\alpha_2 - \alpha_3)) - 3} - \lambda \frac{\sin(\alpha_1 - \alpha_3)}{\sin(\alpha_1 - \alpha_2)} \quad (30)$$

$$\tau_3 = \frac{(2 \cos \alpha_3 - \cos(\alpha_3 - 2\alpha_1) - \cos(\alpha_3 - 2\alpha_2))F_x + (2 \sin \alpha_3 + \sin(\alpha_3 - 2\alpha_1) + \sin(\alpha_3 - 2\alpha_2))(F_y - mg)}{\cos(2(\alpha_1 - \alpha_2)) + \cos(2(\alpha_1 - \alpha_3)) + \cos(2(\alpha_2 - \alpha_3)) - 3} + \lambda \quad (31)$$

To find the feasible region of λ , each wire tension is once set to τ_{min} , minimum allowable tension, and then to τ_{max} , maximum allowable tension and the minimum and maximum values of λ for each wire are calculated. The intersection of the three feasible regions of λ for three wires will be the feasible region of λ for the manipulator. Inside the workspace of the manipulator, this feasible region of λ exists, i.e., $\lambda_{min} < \lambda_{max}$. Outside the workspace of the manipulator, the feasible region of λ does not exist and there is no λ to keep the tension of the three wires in the allowable tension limits. On the boundaries of the workspace, the feasible region of λ reduces to one point, i.e., $\lambda_{min} = \lambda_{max}$.

2.1. Failure of a wire

One type of wire failure is when wire i is disconnected or slack. In this type of failure the i th row of the Jacobian matrix derived in equation (3) and matrix \mathbf{A} in equation (13) are eliminated. For the manipulator studied in this paper, for instance when wire 1 fails, the Jacobian matrix \mathbf{J} and matrix \mathbf{A} reduce to

$$\mathbf{J}_f = - \begin{bmatrix} \cos \alpha_2 & \sin \alpha_2 \\ \cos \alpha_3 & \sin \alpha_3 \end{bmatrix} \quad (32)$$

$$\mathbf{A}_f = \begin{bmatrix} \frac{\sin \alpha_2}{l_2} & -\frac{\cos \alpha_2}{l_2} \\ \frac{\sin \alpha_3}{l_3} & -\frac{\cos \alpha_3}{l_3} \end{bmatrix} \quad (33)$$

After failure of wire 1, the manipulator is no longer redundant and the tension of the remaining wires is calculated as

$$\begin{bmatrix} \tau_2 \\ \tau_3 \end{bmatrix} = \mathbf{J}_f^{-T} \mathbf{F} = \begin{bmatrix} \frac{\sin \alpha_3 F_x - \cos \alpha_3 (F_y - mg)}{\sin(\alpha_2 - \alpha_3)} \\ -\frac{\sin \alpha_2 F_x - \cos \alpha_2 (F_y - mg)}{\sin(\alpha_2 - \alpha_3)} \end{bmatrix} \quad (34)$$

Considering the wire tension limit of $\tau_{\min} \leq \tau_i \leq \tau_{\max}$, the workspace of the manipulator after failure is defined by the following inequalities

$$\tau_{\min} \leq \frac{\sin \alpha_3 F_x - \cos \alpha_3 (F_y - mg)}{\sin(\alpha_2 - \alpha_3)} \leq \tau_{\max} \quad (35)$$

$$\tau_{\min} \leq -\frac{\sin \alpha_2 F_x - \cos \alpha_2 (F_y - mg)}{\sin(\alpha_2 - \alpha_3)} \leq \tau_{\max} \quad (36)$$

The stiffness matrix for the failure case is derived using the differential form of the static force balance equations. As expected, the terms including the tension and stiffness of wire 1 are eliminated. The stiffness matrix is calculated for every position of the mobile platform inside the workspace and to develop the stiffness maps after failure of wire 1.

2.2. Single-dimensional stiffness

For the manipulator studied in this work, the single-dimensional stiffness is defined as the ratio of the 2-norm squared of the force vector \mathbf{F} and the projection of vector \mathbf{F} onto the direction along which the stiffness is sought [13].

$$K_{sd} = \frac{\mathbf{F}^T \mathbf{F}}{\xi^T \mathbf{F}} \quad (37)$$

where vector ξ defines the direction in which the single-dimensional stiffness is calculated. For the considered manipulator, when calculating the stiffness in X and Y directions $\xi = [1, 0]^T$ and $\xi = [0, 1]^T$, respectively. Having the stiffness matrix, the single-dimensional stiffness can be written in terms of the eigenvalues and eigenvectors of the stiffness matrix as

$$K_{sd} = \frac{\sum_{i=1}^n h_i \eta_i \rho_i^T \sum_{i=1}^n h_i \eta_i \rho_i}{\sum_{i=1}^n \eta_i \rho_i^T \sum_{i=1}^n h_i \eta_i \rho_i} \quad (38)$$

where h_i and ρ_i are respectively the i th eigenvalue and eigenvector of the stiffness matrix. Scalar η_i is the

projection of vector ξ onto vector ρ_i , and it is calculated as

$$\eta_i = \xi \cdot \rho_i \quad (39)$$

3. STIFFNESS MAPS

The stiffness matrix of the manipulator shown in Figure 1 is derived before and after the failure, the corresponding single dimensional stiffness is formulated over the manipulator workspace and the stiffness maps are developed. The manipulator is considered to move on the vertical plane (with gravity). The anchor points A_i can move on a circular rail shown by dashed-line in Figure 1 with a radius of 1 m and centered at the origin of the coordinate system $\Psi(X, Y)$ at point 0. For the stiffness maps developed in this section, the coordinates of anchors in terms of their angular positions for a radius of 1 meter are $\{45^\circ, 165^\circ, 285^\circ\}$, i.e., the anchor positions of $(0.7071, 0.7071)$, $(-0.9659, 0.2588)$, $\{(0.2588, -0.9659)\}$ are used. It should be noted that all the length values in this paper are reported in meters. However, these anchor points can be modified, i.e., they can move on the circular rail, to identify the optimum layout of the manipulator in Section 4.

In the simulations, the total mass of mobile platform and payload is $m = 2$ kg. The considered minimum allowable tension in wires is 5 N and the maximum allowable tension is 500 N. The constant length of wire between the motor spool and the pulley is $l_c = 0.3$ m. For the wire actuators, 7×7 wire rope is considered. The cross-section of the wire rope is shown in Figure 2. The wire diameter is 0.0015 m and the wire rope is manufactured from AISI 316 stainless steel grade 1.4401 with $E = 57.3$ GPa [12].

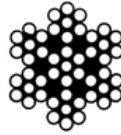


Figure 2. Cross-section of the 7×7 wire rope [12].

Before wire failure, there are infinite possible solutions for the wire tensions in the wire-actuated manipulator. Thus, among possible solutions, the solution corresponding to λ_{max} defined in equation (28) is chosen and used in the stiffness map calculations in this section. This results in maximum possible tension for wires, which satisfies the force balance equations, and maximum stiffness for every position of the mobile platform. Thus, this selection will result in the largest stiffness maps for a required minimum stiffness. Anchor positions are marked with small circles in the figures.

Plots of Figure 3 show the stiffness maps along the X and Y directions, when the force applied on the mobile platform is zero and the manipulator is under the effect of gravity.

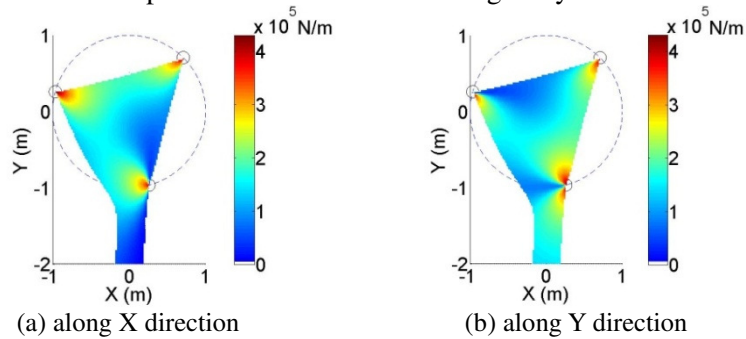


Figure 3. Stiffness maps of manipulator.

Assuming a minimum stiffness of 150 kN/m, the corresponding deflection for the payload of 150 N is 0.001 m. Accuracy in positioning in the order of 0.001 m is reasonable for an assembly task using a manipulator of the size studied in this paper. Stiffness maps of the manipulator for the required minimum stiffness of 150 kN/m are shown in Figure 4.

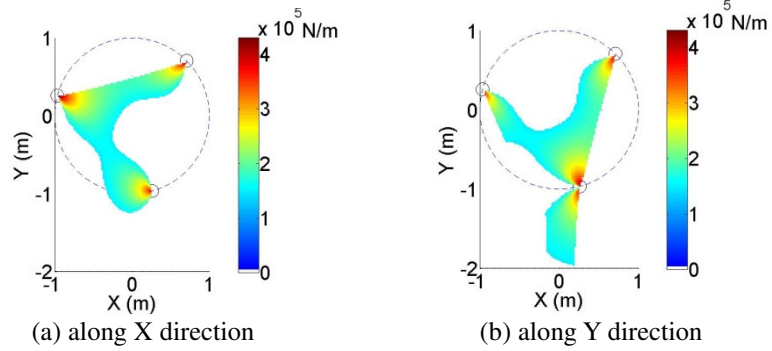


Figure 4. Stiffness maps of manipulator for the required minimum stiffness.

Plots of Figure 5 show the stiffness maps of the manipulator after failure of wire 1. In addition, stiffness maps of the manipulator after failure of wire 1 for the required minimum stiffness of 150 kN/m are shown in Figure 6.

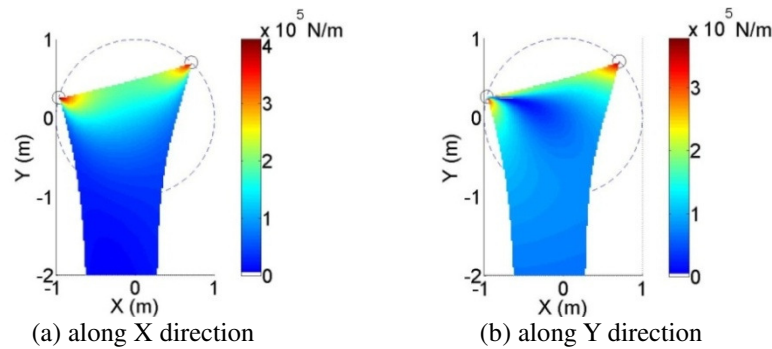


Figure 5. Stiffness maps of manipulator after failure of wire 1.

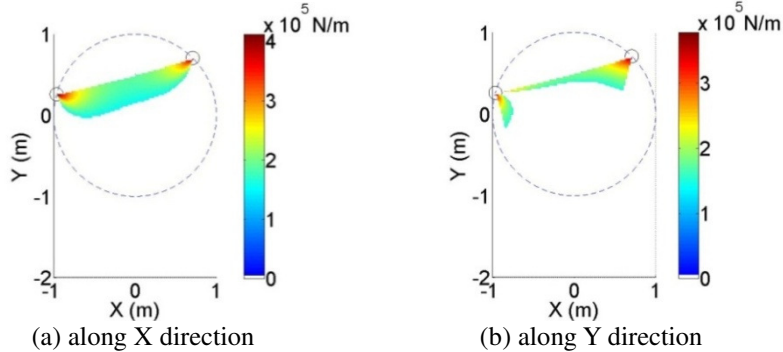


Figure 6. Stiffness maps of manipulator for the required minimum stiffness after failure of wire 1.

Comparing plots of Figure 6 and Figure 4, it can be seen that the stiffness maps shrink drastically after failure.

4. OPTIMUM LAYOUTS OF MANIPULATOR

In this section, anchor positions of the manipulator are optimized to maximize the stiffness map area. In other words, the optimum layout of the manipulator is identified to maximize the area of the stiffness maps considering the constraint that the anchor positions should be on the circular rail shown in Figure 1. The stiffness maps for the optimum layouts of the manipulator are developed with and without the required minimum stiffness and also before and after failure.

The wire tension constraints are checked for each potential position of mobile platform to identify the workspace before and after failure. For all the positions of the mobile platform inside the workspace, the

stiffness matrix is derived following the procedure discussed in Section 2. After deriving the stiffness map, the number of poses inside the map corresponds to the area of the stiffness map.

The expressions for the boundaries of the stiffness maps in terms of the anchor positions are quite lengthy. To identify the optimum anchor positions parametrically, the parametrical expression for the area of the stiffness map needs to be formulated which is not easily obtainable. Thus, for each case, the optimization is carried out in MATLAB using the *genetic algorithm* (GA) function to identify the optimum anchor positions that maximize the stiffness map area. It should be noted that the area of the stiffness map is calculated numerically for each case. After deriving the stiffness map, the number of poses inside the map corresponds to the area of the stiffness map. This integer number can be converted to the area of the stiffness map knowing that the increment of 0.02 m in generating the poses in X and Y directions is considered. GA is a stochastic optimization algorithm that was originally motivated by the mechanisms of natural selection and evolutionary genetics [14, 15]. Parameters used in the GA function are listed in Table 1.

Table 1. GA function parameters

GA function variable	value
Population size	20
Generations	100
Migration fraction	0.2
Crossover fraction	0.8
Initial penalty	10
Penalty factor	100
TolFun	10^{-6}

The parameters in Table 1 are defined as follows. An individual is a single solution to the optimization problem which is the anchor position here. A population is an array of individuals and population size is the number of individuals in each population. At each iteration, the genetic algorithm performs a series of computations on the current population to produce a new population. Each successive population is called a new generation. Number of generations specifies the maximum number of iterations before the algorithm halts. In this optimization problem it has also been set that the algorithm runs until the cumulative change in the fitness function value over the last 50 generations is less than TolFun. The next generation is made of the individuals that are guaranteed to survive from the previous generation (elite children) and the individuals made by crossover. Crossover is the process of combining two individuals, or parents, to form a crossover child for the next generation. The crossover fraction specifies the fraction of the next generation, other than elite children, that are produced by crossover. Migration is the process that the best individuals from one subpopulation replace the worst individuals in another subpopulation. The migration fraction is a scalar between 0 and 1 specifying the fraction of individuals in each subpopulation that migrates to a different subpopulation. When the constraints are violated in the optimization, the solution is not feasible. Thus, a penalty or cost is associated with all constraint violations to eliminate them from the population in the next generations. Initial penalty specifies an initial value of the penalty parameter that is used by the algorithm. Initial penalty must be greater than or equal to 1. The penalty factor increases the penalty parameter when the problem is not solved to the required accuracy and the constraints are not satisfied. In this optimization problem, the goal is to maximize the stiffness map area with the constraint that the anchor positions should be on a circular rail with the radius of 1 m and centered at point 0. The optimum anchor positions for the manipulator before failure and when the mobile platform is under the effect of gravity have been identified as $\{(0.9999, 0.0048), (-0.9984, -0.0566), (-0.0334, 0.9994)\}$ and the value of the optimum stiffness map area is 3.3502 m^2 . The whole number values for the anchor positions, i.e., $\{(1, 0), (-1, 0), (0, 1)\}$, have also been checked but this would result in a slightly smaller stiffness map area of 3.3438 m^2 . Thus, the optimum anchor positions are used and the stiffness maps for this optimum layout are shown in Figure 7. It should be noted that in

calculating and comparing these values of the stiffness map areas, the finer resolution of 0.005 m in generating the poses in X and Y directions is considered.

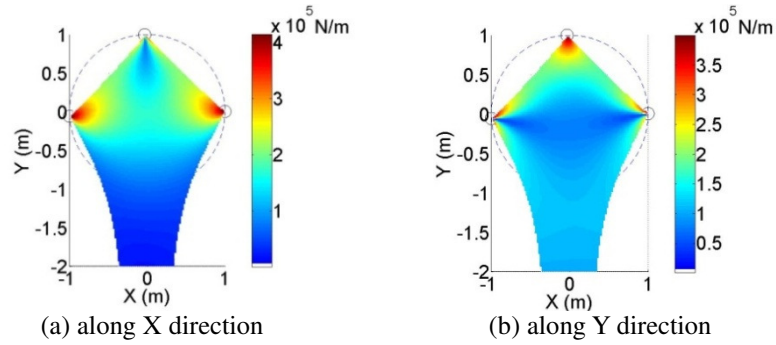


Figure 7. Stiffness maps of the manipulator with the optimum layout.

The optimum anchor positions for the manipulator before failure for the required minimum stiffness of 150 kN/m have been identified as $\{(-0.4524, -0.8918), (-0.9991, 0.0423), (0.9788, 0.2049)\}$ for the stiffness along X direction and $\{(-0.2476, -0.9689), (0.9397, 0.3421), (-0.1050, 0.9945)\}$ for the stiffness along Y direction. The stiffness maps for these optimum layouts are shown in Figure 8. Optimum anchor positions for the case that the stiffness in both X and Y directions are over 150 kN/m are $\{(-0.9939, -0.1100), (0.9999, 0.0119), (0.0707, 0.9975)\}$. This optimum layout and its stiffness maps are shown in Figure 9.

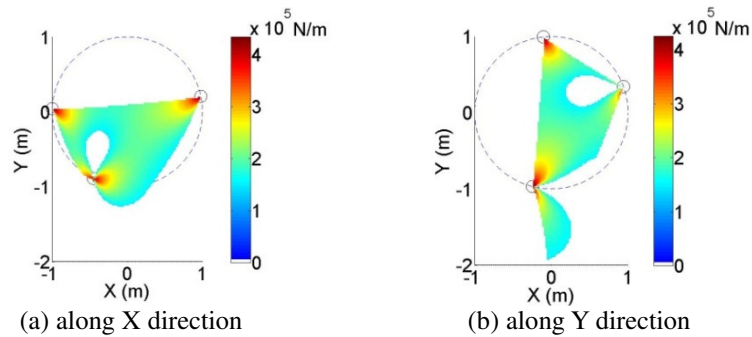


Figure 8. Stiffness maps of the manipulator for the required minimum stiffness with the optimum layout.

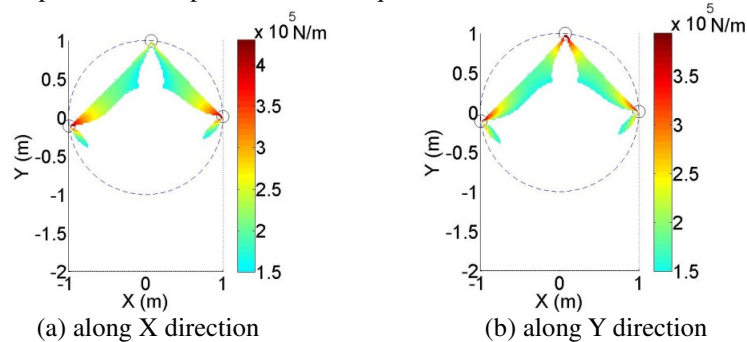


Figure 9. Stiffness maps of the manipulator with the optimum layout for the required minimum stiffness in both X and Y directions.

The optimum anchor positions for the manipulator after failure of a wire have been identified as $\{(-0.9769, 0.2135), (0.9819, 0.1892)\}$ and the value of the optimum stiffness map area is 3.2013 m^2 . The whole number values for the anchor positions, i.e., $\{(-1, 0), (1, 0)\}$, have also been checked but this

would result in a slightly smaller stiffness map area of 3.0433 m^2 . Thus, the optimum anchor positions are used and the stiffness maps for this optimum layout are shown in Figure 10.

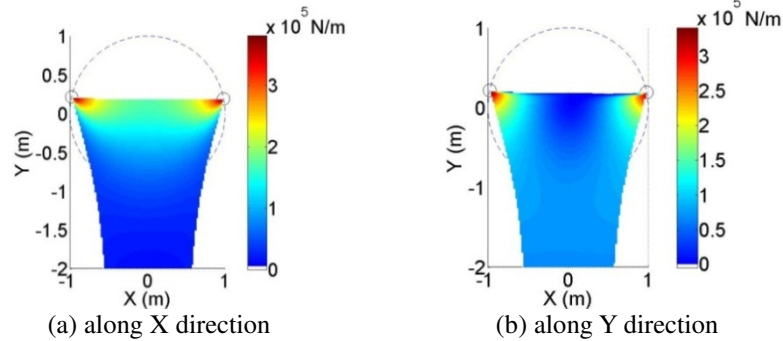


Figure 10. Stiffness maps of the manipulator after failure of a wire with the optimum layout.

The optimum anchor positions for the minimum stiffness of 150 kN/m after failure of a wire have been identified as $\{(-0.9960, 0.0897), (0.9974, 0.0717)\}$ for the stiffness along X direction and $\{(-0.0114, 0.9999), (0.9999, 0.0017)\}$ for the stiffness along Y direction. These anchor positions are different than the optimum layouts shown in Figure 8 before failure because after the failure, the manipulator works with 2 wires under the effect of gravity. Similar to the previous cases, the whole number values for the anchor positions, i.e., $\{(-1, 0), (1, 0)\}$ and $\{(1, 0), (0, 1)\}$, would result in slightly smaller stiffness map areas. Thus, the optimum anchor positions are used and the stiffness maps for these optimum layouts are shown in Figure 11. Optimum anchor positions for the case that the stiffness in both X and Y directions are over 150 kN/m are $\{(-0.3699, 0.9291), (0.9999, 0.0047)\}$. This optimum layout and its stiffness maps are shown in Figure 12.

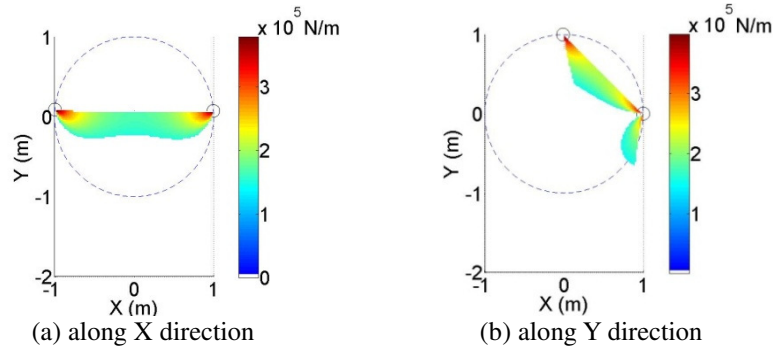


Figure 11. Stiffness maps of the manipulator for the required minimum stiffness after failure of a wire with the optimum layout.

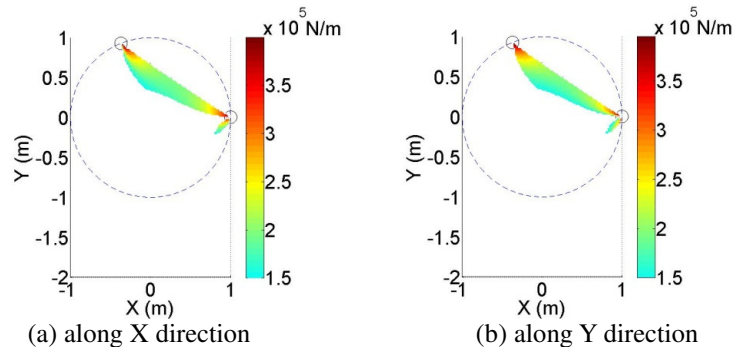


Figure 12. Stiffness maps of the manipulator after failure of a wire with the optimum layout for the required minimum stiffness in both X and Y directions.

Comparing the stiffness maps before optimization with the corresponding stiffness maps after optimization, it can be seen that the area of the stiffness maps have been increased after optimizing the layout of the manipulator.

5. DISCUSSION AND CONCLUSIONS

In this article, the complete form of the stiffness matrix of 2-DOF planar three-wire-actuated parallel manipulator was formulated parametrically. Using the differential form of the static force balance equations for a given position of the manipulator, the stiffness of the manipulator after failure of a wire was modelled. Single-dimensional stiffness maps of the manipulator before and after failure, also with and without a required minimum stiffness were developed and the effect of the manipulator layout on the stiffness map area was investigated. Optimum layouts to maximize the area of the stiffness maps were identified and the corresponding stiffness maps were developed. The optimum layouts for the manipulator can be used when designing the manipulator. This knowledge can be used in control of the manipulator to retrieve the lost stiffness after failure partially and to achieve a better fault tolerant manipulator.

REFERENCES

- [1] C. Won, H. Kino, K. Katsuta and S. Kawamura, "A design of parallel wire driven robots for ultrahigh speed motion based on stiffness analysis," in *Proc. of the Japan-USA Symposium on Flexible Automation*, vol.1, pp. 159-166, 1996.
- [2] X. J. Liu, Z. L. Jin and F. Gao, "Optimum design of 3-DOF spherical parallel manipulators with respect to the conditioning and stiffness indices," *Mechanism and Machine Theory*, vol. 35, no.9, pp. 1257-1267, 2000.
- [3] M. Azadi, S. Behzadipour and G. Faulkner, "Antagonistic variable stiffness elements," *Mechanism and Machine Theory*, 44(9):1746-1758, 2009.
- [4] S. Chen and I. Kao, "Conservative congruence transformation for joint and Cartesian stiffness matrices of robotic hands and fingers," *International Journal of Robotics Research*, vol. 19, no.9, pp. 835-847, 2000.
- [5] S. Sahin and L. Notash, "Force and stiffness analysis of wire-actuated parallel manipulators," in *Proc. of 12th World Congress in Mechanism and Machine Science*, 2007.
- [6] T. Pigoski, M. Griffis and J. Duffy, "Stiffness mappings employing different frames of reference," *Mechanism and Machine Theory*, vol. 33, no.6, pp. 825-838, 1998.
- [7] J. Kovecses and J. Angeles, "The stiffness matrix in elastically articulated rigid-body systems," *Multibody System Dynamics*, vol. 18, no.2, pp. 169-184, 2007.
- [8] L. Notash, and L. Huang, "On the Design of Fault Tolerant Parallel Manipulators," *Mechanism and Machine Theory*, 38(1):85-101, 2003.
- [9] L. Notash, "A Failure Recovery Methodology for Wire-Actuated Parallel Manipulators," *Proc. of CSME Forum*, Victoria, 8 pages, June 2010.
- [10] P. Bosscher and I. Ebert-Uphoff, "Wrench-Based Analysis of Cable-Driven Robots," *Proc. of IEEE International Conference on Robotics & Automation (ICRA '04)*, New Orleans, 6 pages, 2004.
- [11] A. Moradi and L. Notash, "Investigation of Wire Failure Effect on Stiffness Maps of Planar Wire-Actuated Parallel Manipulators," *Proc. of ASME 34th Annual Mechanisms and Robotics Conference (IDETC/CIE 2010)*, Montreal, 8 pages, 2010.
- [12] S3i Ltd., <http://www.s3i.co.uk/wire-rope-technical.php>, accessed April 6, 2011.
- [13] B. S. El-Khasawneh and P. M. Ferreira, "Computation of stiffness and stiffness bounds for parallel link manipulators," *International Journal of Machine Tools & Manufacture*, vol. 39, no.2, pp. 321-342, 1999.
- [14] D.E. Goldberg, "Genetic algorithms in search, optimization, and machine learning," Massachusetts : Addison-Wesley Publishing Company, 1989.
- [15] S.N. Sivanandam and S.N. Deepa, "Introduction to genetic algorithms," New York : Springer, 2007.